ChemPubSoc Europe
DOI: 10.1002/cssc.201600785
CHEMSUSCHEM Communications

Low Pt-Loaded Mesoporous Sodium Germanate as a High-Performance Electrocatalyst for the Oxygen Reduction Reaction

Xiaoxia Zhou,[a] Lisong Chen,[a] Gang Wan,[a] Yu Chen,[a] Qinglu Kong,[a] Hangrong Chen,*[a, b] and Jianlin Shi*[a, b]

Although Pt/C catalysts show relatively high activities for the oxygen reduction reaction (ORR) and great potential for use in polymer electrolyte membrane fuel cells, the large amount of Pt required and the poor stability of Pt/C-based catalysts remain big challenges. Herein, mesoporous $Na_4Ge_9O_{20}$ microcrystals have been successfully synthesized to serve as a new kind of electrocatalyst support owing to its special structural characteristics and high structural stability. After loading a low amount of Pt (5 wt%) nanoparticles of 2–5 nm in diameter, the obtained mesoporous Pt/$Na_4Ge_9O_{20}$ composite shows not only high electrocatalytic activity for ORR in both acidic and alkaline electrolyte media, which are comparable to those of conventional 20 wt% Pt/C, but also remarkably enhanced Pt mass-specified ORR current density and durability. Synergetic catalytic effects between loaded Pt and the support for the ORR activity has been proposed.

Polymer electrolyte membrane fuel cells (PEMFCs) have been becoming one of the most promising green energy sources to replace traditional ones on a large scale.[1,2] However, extensive application of fuel cells is hindered owing to electrochemical stability and high Pt loading required for the commercial Pt/C catalyst used for the oxygen reduction reaction (ORR) at the cathodes. Therefore, the exploration of highly active and electrochemically stable catalysts with minimal Pt loading for ORR has received much attention in recent years. Many kinds of active Pt-based metal alloys have been developed to reduce the Pt usages, such as the Pt-Ni,[3,4] core-shell Pd@PtNi nanoparticles,[5] Pt skin-layer,[6,7] and thin films,[8,9] which shows the unique electrocatalytic activity toward ORR. Besides, carbon-based electrocatalysts (i.e., N/B-doped carbon nanotubes,[10,11] Co_3O_4 loaded graphene[12] and N/S/P-doped graphene[13–15]) are promising alternatives to Pt-based catalysts for ORR, which also show better electrochemical stability as well as good ORR activity. Additionally, it is noted that the spinels as an alternative low-cost bifunctional electrocatalyst have been developed rapidly in the recent years [e.g., $M_xMn_{3-x}O_4$ (M = divalent metals)[16] and $MMoO_4$ (M = Co, Ni, or Fe)[17]] and exhibits excellent oxygen reduction and/or evolution reaction (ORR/OER) activity.

A series of germanate crystals $M_4Ge_9O_{20}$ (M = Na, K) as a potential and important semiconductor and infrared material, were usually synthesized under harsh hydrothermal conditions (i.e., under a pressure of 0.05 GPa and at a high temperature of 350 °C).[18] The $M_4Ge_9O_{20}$ crystal contains tetrahedral [GeO_4] and octahedral [GeO_6] units, indicating that germanate has richer topology structure than silicate. As far as we know, the $M_4Ge_9O_{20}$ crystal as an electrocatalyst support has never been reported. Compared with carbon-based materials, $M_4Ge_9O_{20}$ features the following structural characteristics favoring its use as a support for ORR: 1) the rich topology structure as well as the porous structure enables fast diffusion and transport of the reactants and products, 2) the highly crystalline framework of $M_4Ge_9O_{20}$ endows the material with higher tolerance to acid and basic corrosion than commercial carbon materials, and 3) the germanate $M_4Ge_9O_{20}$ possesses abundant vacancies owing to the doping of the low valence heteroatom M, which is helpful to the adsorption and activation of O_2. Additionally, it has also been found that nanocomposites of semiconductors and precious metals can bring about unique physical and chemistry features through strong metal–substrate coupling interactions,[19,20] which may create opportunities in the development of functionalized catalytic materials for applications in clean energy and environmental protections.[21–23] Therefore, it is possible to achieve substantially improved ORR performances by designing and fabricating a nanocomposite of precious metal-loaded germanate crystal $M_4Ge_9O_{20}$.

Herein, mesoporous $Na_4Ge_9O_{20}$ is used as an electrocatalyst support for ORR, for the first time. The material was successfully synthesized under mild hydrothermal conditions assisted by tetraethylammonium hydroxide. Then, a highly active and stable electrochemical catalyst was obtained by further loading a low amount of Pt nanoparticles on the synthesized support. The obtained nanocomposite Pt(5 wt%)/$Na_4Ge_9O_{20}$ exhibits excellent catalytic activity and high durability for ORR in both acidic and alkaline electrolyte solutions, which are comparable to the commercial carbon-supported Pt catalyst (20 wt% Pt/C).

XRD patterns shown in Figure S1 confirm that the prepared catalyst support well corresponds to the $Na_4Ge_9O_{20}$ crystals

[a] X. Zhou, L. Chen, G. Wan, Y. Chen, Q. Kong, Prof. Dr. H. Chen, Prof. Dr. J. Shi
State Key Laboratory of High Performance Ceramics and Superfine Microstructures
Shanghai Institute of Ceramics
Chinese Academy of Science
No. 1295 Ding-xi Road, Shanghai 200050 (P.R. China)
Fax: (+86) 21-5241-3122
E-mail: hrchen@mail.sic.ac.cn
jlshi@mail.sic.ac.cn

[b] Prof. Dr. H. Chen, Prof. Dr. J. Shi
Jiangsu National Synergetic Innovation Center for Advanced Materials

Supporting Information for this article can be found under: http://dx.doi.org/10.1002/cssc.201600785.

(JCPDS: 80-0703). After loading the Pt, the Pt/$Na_4Ge_9O_{20}$ sample shows the $Na_4Ge_9O_{20}$ characteristic diffraction with a little lower intensity, and no Pt diffraction peaks can be detected, suggestive of low loading amount of Pt and/or small Pt particle sizes with weak crystallization. The N_2 adsorption isotherms for $Na_4Ge_9O_{20}$ and Pt/$Na_4Ge_9O_{20}$ are shown in Figure S2 and the corresponding pore structure parameters are summarized in Table S1. Two samples exhibit typical type IV isotherms, confirming the presence of mesoporous structure owing to aggregation of $Na_4Ge_9O_{20}$ nanoparticles. The pore structure parameters of the $Na_4Ge_9O_{20}$ are nearly unchanged after loading the Pt species, and the Brunauer–Emmett–Teller (BET) surface area, mesoporous volume, and pore size are 69 $m^2 g^{-1}$, 0.06 $cm^3 g^{-1}$, and 3.4 nm, respectively. The field emission SEM (FE-SEM) and low-magnification TEM images, shown in Figure 1 a–b, reveal that the $Na_4Ge_9O_{20}$ is composed of micrometer-sized and irregularly shaped crystals, and the FE-SEM image further indicates that the mesopore structure comes from the accumulation of nanocrystals. The high-resolution TEM (HR-TEM) image (Figure 1 c) clearly exhibits the lattice fringes of crystals $Na_4Ge_9O_{20}$, and the corresponding selected area electron diffraction (SAED) pattern in the inset of Figure 1 c confirms that the prepared $Na_4Ge_9O_{20}$ has a single crystalline character. The typical FE-SEM and HR-TEM images of Pt/$Na_4Ge_9O_{20}$ are shown in Figure 1 d–e; it can be found that Pt nanoparticles are uniformly dispersed onto the support $Na_4Ge_9O_{20}$ without apparent aggregation (Figure 1 d) and the diameter of Pt is smaller than 5 nm. In addition, the Pt nanoparticles are found in the HR-TEM image (Figure 1 e), as indicated by the yellow arrows. The Pt loading amount is 5.0 wt% measured by the inductively coupled plasma atomic emission spectroscopy (ICP-AES). The corresponding energy dispersive X-ray spectroscopy (EDX) spectrum and its quantitative result confirm the existence of Pt and give a similar Pt content to the ICP-AES result (Figure 1 f).

The UV/Vis diffuse reflectance spectrum of $Na_4Ge_9O_{20}$ shows typical optical characteristics of semiconductors. Figure S3 suggests that the absorption edge for the $Na_4Ge_9O_{20}$ is about 359 nm, and the indirect bandgap is 2.75 eV.

Figure S4 shows the XPS analysis results of the sample Pt/$Na_4Ge_9O_{20}$. The O 1s XPS peak of Pt/$Na_4Ge_9O_{20}$ can be deconvoluted into two components at 530.5 and 532.2 eV after Gaussian fitting, which can be ascribed to lattice oxygen O_L and surface adsorbed oxygen O_C, respectively. Besides, as high as 59.5% (Table S2) of surface adsorbed oxygen O_C is seen in the Pt/$Na_4Ge_9O_{20}$ sample, which is related to Pt–O or Ge–O species.[24,25] The binding energy of the Pt $4f_{7/2}$ at 71.3 and 72.2 eV can be assigned to the Pt and PtO signals,[24,26] which accounts for 32.5% and 67.5% of the total Pt content, respectively (Figure S4 b and Table S2). It is believed that the co-existence of Pt and PtO in the sample Pt/$Na_4Ge_9O_{20}$ would be favorable in elevating the ORR catalytic activity. It is noted that compared to the bulk metal Pt at 70.8 eV, Pt/$Na_4Ge_9O_{20}$ shows a slight shift to higher energy, which can be ascribed to the interaction between the catalyst support and the loading Pt species.

The ORR eletrocatalytic activity of prepared support $Na_4Ge_9O_{20}$ was investigated in N_2- and O_2-saturated 0.1 M KOH electrolyte solution using cyclic voltammetry (CV), as shown in Figure S5 a. The CV curve of $Na_4Ge_9O_{20}$ shows a featureless voltammetric profile in N_2-saturated KOH electrolyte solution in

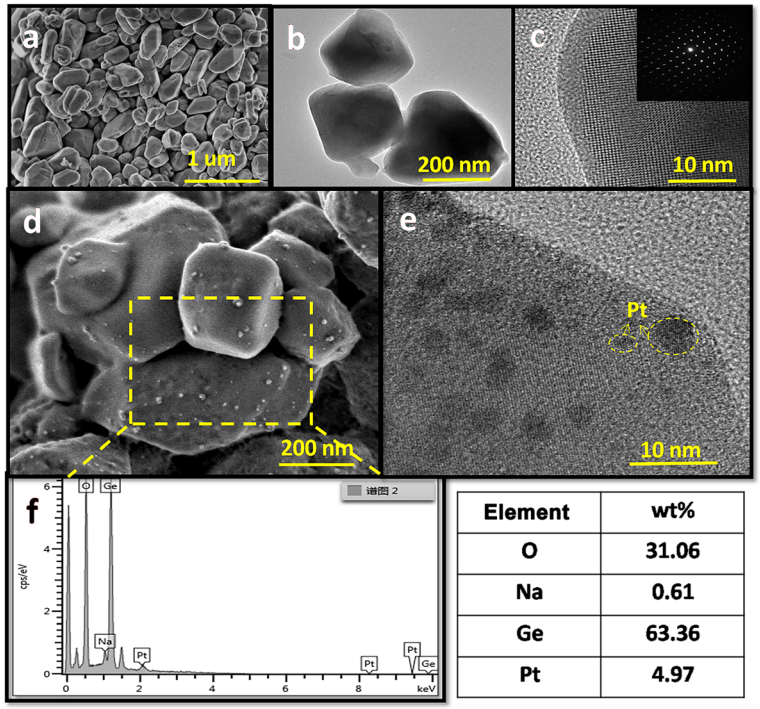

Element	wt%
O	31.06
Na	0.61
Ge	63.36
Pt	4.97

Figure 1. a) Typical FE-SEM. b) Low-magnification and c) HR-TEM images of $Na_4Ge_9O_{20}$. d–e) FE-SEM and HR-TEM images of the Pt/$Na_4Ge_9O_{20}$. f) The corresponding EDX spectrum to the selected area in d and its quantitative result.

the potential range of −1.0 to 0 V. In contrast, the electrodes exhibit a dramatic increase in voltammetric current in O_2-saturated alkaline solution, with a relatively positive ORR onset potential (−0.29 V vs. Ag/AgCl) and a high cathodic current density (−0.72 mA cm^{-2}). The linear sweep voltammograms (LSV) of $Na_4Ge_9O_{20}$ in alkaline medium using a rotating disk electrode (RDE) are shown in the Figure S5 b, and a two-step transfer pathway by producing HO_2^- as intermediates is observed. Furthermore, the rotating ring-disk electrode (RRED) measurements (Figure S5 c) also show high ring currents of the $Na_4Ge_9O_{20}$. The electron transfer number (*n*) is 2.2–2.5 for $Na_4Ge_9O_{20}$ from −0.3 to −1.0 V on the basis of the ring and disk currents (Figure S5 d), indicating a dominant two-electron process.

Interestingly, the ORR performance of the $Na_4Ge_9O_{20}$ by loading a low amount of precious metal (5 wt% Pt) can be greatly enhanced in 0.1 M KOH electrolyte solution, and the CV curve of Pt/$Na_4Ge_9O_{20}$ shows a more positive ORR onset potential (−0.04 V vs. Ag/AgCl) and a higher current density (−1.02 mA cm^{-2}) than that of support $Na_4Ge_9O_{20}$, as shown in Figure 2 a. RDE measurement results indicate a four-electron transfer pathway and the half-wave potential is −0.20 V vs. Ag/AgCl at 1600 rpm (Figure 2 b), similar to that of 20 wt% Pt/C (−0.16 V, Figure S6 a). The results of the Tafel plot (Figure 2 c), based the analysis the LSV curves, indicate a higher slope for the Pt/$Na_4Ge_9O_{20}$ (83 mV dec^{-1}) in the lower overpotential region than the reference Pt/C (60 mV dec^{-1}), suggesting the relatively slow kinetics for ORR in alkaline electrolyte solution, which is related to the relatively weak conductivity of the support $Na_4Ge_9O_{20}$. However, the corresponding Koutecky–Levich (K–L) plots at different potentials exhibit good linearity (Figure 2 d), and the slopes keep constant from −0.60 to −0.90 V vs. Ag/AgCl, implying the similar *n*. Moreover, the *n* is 3.8 by calculating from the K–L equation, indicating the catalyst Pt/$Na_4Ge_9O_{20}$ follows the four-electron reduction mechanism in the ORR. In addition, the *n* of the Pt/$Na_4Ge_9O_{20}$ in alkaline electrolyte solution is 3.6–3.8 over the potential range of −0.6 to −0.9 V vs. Ag/AgCl (inset in Figure 2 e) based on the corresponding RDE dates, which is basically consistent with the results of K–L plots analysis. The RDE measurements (Figure 2 e) are conducted to verify the formation of the intermediates HO_2^-, and the HO_2^- yield is as low as 3% for Pt/$Na_4Ge_9O_{20}$, as

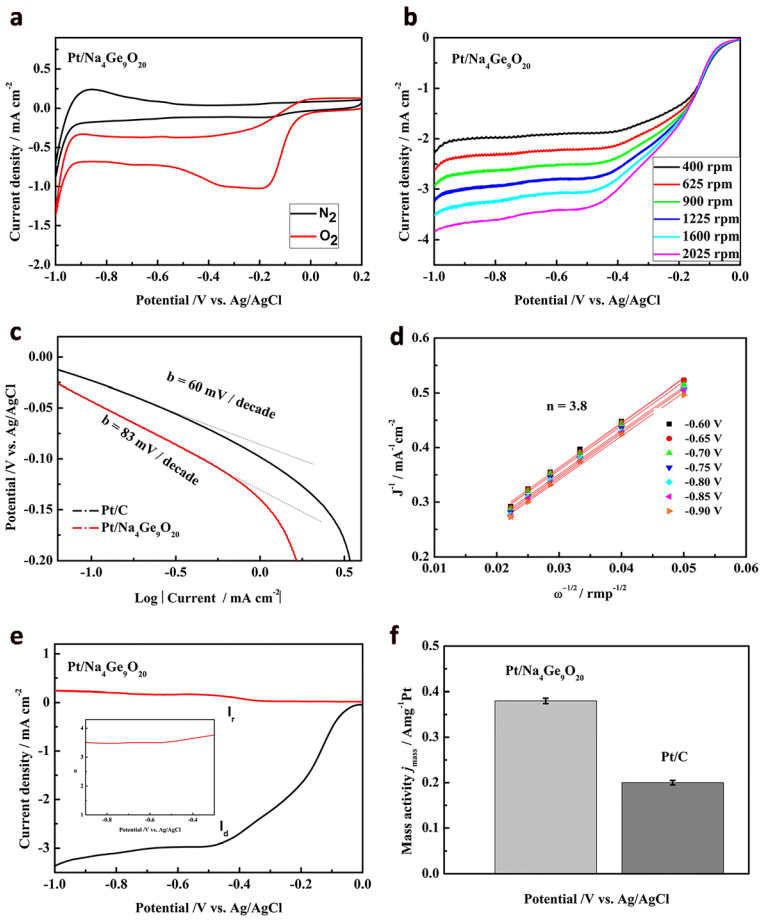

Figure 2. The electrocatalytic activity for ORR in KOH electrolyte solutions (0.1 M). a) CV traces of Pt/$Na_4Ge_9O_{20}$ at a scan rate of 100 mV s^{-1}. b) LSV scans on Pt/$Na_4Ge_9O_{20}$ in O_2-solution at a scan rate of 10 mV s^{-1} and different rotation rates. c) Tafel plots of Pt/$Na_4Ge_9O_{20}$ and Pt/C at a rotation rate of 1600 rpm. d) K–L plots at different potentials. e) RRED test of the ORR on the Pt/$Na_4Ge_9O_{20}$ in O_2-saturated electrolyte solution at a rotation rate of 1600 rpm. The dark potential was scanned at 10 mV s^{-1} while the ring potential was fixed at 0.5 V vs. Ag/AgCl during the tests (I_r: ring current; I_d: disc current). inset) The *n* of Pt/$Na_4Ge_9O_{20}$ at varied potentials based on the corresponding RRED dates. f) Mass-specified ORR current density (j_{mass}) of Pt/$Na_4Ge_9O_{20}$ and commercial Pt/C at an electrode rotating rate of 1600 rpm and a potential of −0.1 V vs. Ag/AgCl.

shown in Figure S7a, indicating a dominant four-electron process. More importantly, the mass-specified kinetic current densities (j_{mass}) are 0.38 A mg^{-1} Pt and 0.20 A mg^{-1} Pt for the sample Pt/$Na_4Ge_9O_{20}$ and the commercial Pt/C at −0.1 V vs. Ag/AgCl, respectively. The former is twice that of the later, as shown in Figure 2 f, which is highly encouraging for the future PEMFC application of the synthesized Pt/$Na_4Ge_9O_{20}$.

More encouragingly, the Pt/$Na_4Ge_9O_{20}$ sample also shows an excellent ORR performance in acidic electrolyte solution (0.1 M $HClO_4$). The CV curve of Pt/$Na_4Ge_9O_{20}$ exhibits a more positive ORR onset potential (0.62 V) and a higher current (−1.23 mA cm^{-2}) in the O_2-saturated $HClO_4$ electrolyte solution, as shown in Figure 3 a. Compared to the commercial 20 wt% Pt/C (Figure S6 b), the half-wave potential for the Pt/$Na_4Ge_9O_{20}$ has a slight shift of 10 mV towards the positive direction [i.e., 0.46 V vs. Ag/AgCl at 1600 rpm (Figure 3 b)], suggesting largely accelerated ORR reaction kinetics. The ORR kinetics investigation of the Pt/$Na_4Ge_9O_{20}$ by Tafel analysis in the low overpotential region indicates a comparable ORR activity (104 m dec^{-1}) compared to the Pt/C (102 mV dec^{-1}), as shown in Figure 3 c, suggesting a quick ORR kinetics in acidic electrolyte solution. By the polarization curves, several potential points from 0.00–0.50 V vs. Ag/AgCl are also chosen to determine the K–L slope and calculate n (Figure 2 d). The n was determined to be 3.9, confirming a highly desirable four-electron reduction pathway in the ORR. In addition, the RRED measurements (Figure 3 c) are also performed to determine the ORR catalytic pathway and monitor the formation of H_2O_2 of the Pt/$Na_4Ge_9O_{20}$ sample in the ORR process.[27] It is noted that the amount of produced H_2O_2 species is lower than 2% (Figure S7 b) over the sample Pt/$Na_4Ge_9O_{20}$, giving a n of 3.9 (inset in Figure 3 c) in acidic electrolyte solution, which is consistent with the analysis of K–L plots, indicating a dominant four-electron process. More importantly, the mass activity of Pt/$Na_4Ge_9O_{20}$ has been calculated to be 0.15 A mg^{-1} Pt at 0.6 V vs Ag/AgCl, which is remarkably higher than that of the commercial catalyst Pt/C (0.035 A mg^{-1} Pt), indicating a great enhancement of electrochemical ORR activity in the acidic electrolyte solution.

To better understand the transport property of electrons on Pt/$Na_4Ge_9O_{20}$, electrochemical impedance spectroscopy (EIS) characterization was performed under dark conditions, as

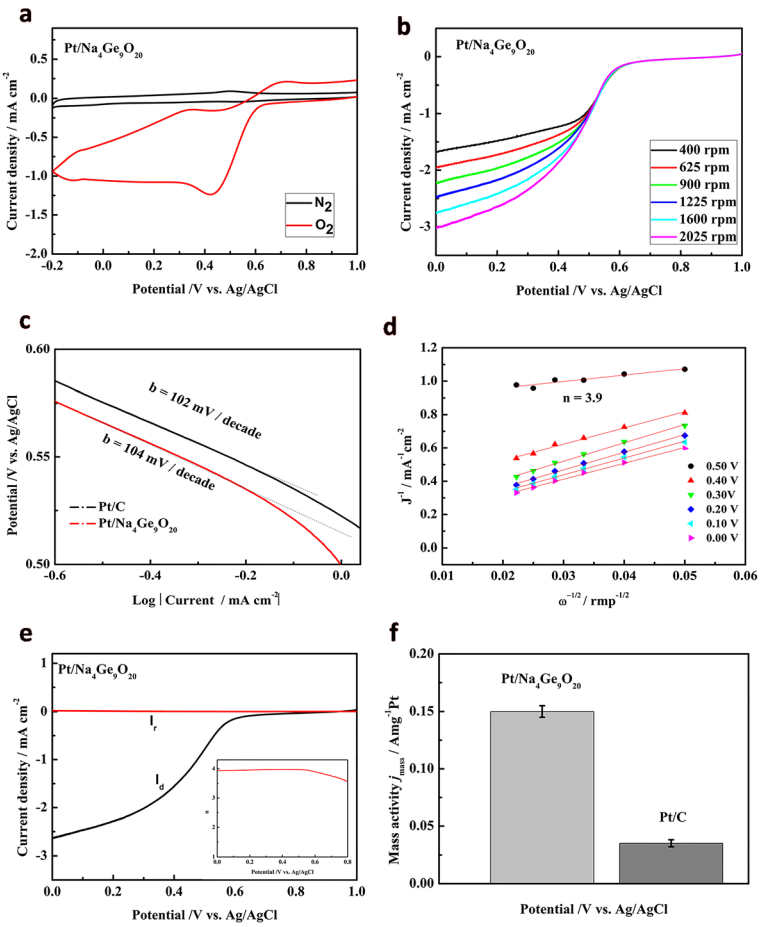

Figure 3. The electrocatalytic activity for ORR in 0.1 M $HClO_4$ electrolyte solution. a) CV scans of Pt/$Na_4Ge_9O_{20}$ in N_2- and O_2-saturated solutions at a scan rate of 100 mV s^{-1}. b) LSV scans on the Pt/$Na_4Ge_9O_{20}$ in O_2-saturated electrolyte solution at a scan rate of 10 mV s^{-1} and different rotation rates. c) Tafel plots of Pt/$Na_4Ge_9O_{20}$ and Pt/C at a rotation rate of 1600 rpm. d) K–L plots at different potentials. e) RRED tests of the ORR on the Pt/$Na_4Ge_9O_{20}$ in O_2-saturated $HClO_4$ electrolyte solution (0.1 M) at a rotation rate of 1600 rpm. The dark potential was scanned at 10 mV s^{-1} while the ring potential was fixed at 0.5 V vs. Ag/AgCl during the tests. inset) The n of Pt/$Na_4Ge_9O_{20}$ at varied potentials based on the corresponding RRED data. f) Pt mass-specified ORR current density (j_{mass}) of Pt/$Na_4Ge_9O_{20}$ and commercial Pt/C with the rotating rate of 1600 rpm at 0.6 V vs. Ag/AgCl.

shown in Figure S8. It is found that both the $Na_4Ge_9O_{20}$ and Pt/$Na_4Ge_9O_{20}$ show a semicircle in the high frequency region at 1.2 V, and the diameter of the semicircle of Pt/$Na_4Ge_9O_{20}$ is smaller than that of $Na_4Ge_9O_{20}$, which indicates that the electron/charge transfer resistance of Pt/$Na_4Ge_9O_{20}$ is much smaller than the support $Na_4Ge_9O_{20}$ and the higher electrical conductance of Pt/$Na_4Ge_9O_{20}$ can lead to the faster reaction rate in the ORR.

The long-term durability of Pt/$Na_4Ge_9O_{20}$ was evaluated by stability tests, as shown in Figure S9. The results demonstrate that the new Pt/$Na_4Ge_9O_{20}$ electrocatalyst displays excellent long term stability not only in the alkaline solution also in the acidic medium. It is found that the half-wave potential for the Pt/$Na_4Ge_9O_{20}$ remains almost unchanged both in the alkaline and acidic electrolyte solutions at the 2000th LSV cycle at 50 mV s^{-1}. Additionally, the half-wave potentials for the Pt/$Na_4Ge_9O_{20}$ decay by only 15 (Figure S9 a) and 20 mV (Figure S9 b) in the alkaline and acidic electrolyte solutions at the 5000th cycle, respectively. For comparison, the commercial Pt/C shows 15 and 21 mV negative shifts in the alkaline electrolyte solution, and 20 and 60 mV in the acidic electrolyte solution, in the half-wave ORR potentials at 2000th and 5000th cycles, respectively, as shown in Figure S10. The above durability tests confirm the extremely promising electrochemical stability of such a novel kind of electrocatalyst Pt/$Na_4Ge_9O_{20}$ in both alkaline and acidic media, resulting from the high structural stability of the Pt/$Na_4Ge_9O_{20}$ and high dispersion of nanoparticles Pt in the support $Na_4Ge_9O_{20}$.

A possible catalytic mechanism toward ORR over the Pt/$Na_4Ge_9O_{20}$ in alkaline and acidic media is proposed, and two possible four-electron reaction pathways are shown in Scheme 1. Firstly, a large amount of intrinsic oxygen vacancies can be generated in the lattice of the support $Na_4Ge_9O_{20}$ owing to the doping of the heteroatom Na among [GeO_4] and [GeO_6] groups, as shown in step 1 in Scheme 1. Therefore, O_2 molecules in the electrolyte solution can be adsorbed quickly (O_{ads}) onto the surface of the support and then further activated to form the activated oxygen (O*). The O* species will migrate to Pt nanoparticles along the surface of the $Na_4Ge_9O_{20}$ and be reduced to OH^- in alkaline media through the four-electron ORR reaction $2\,Pt{-}O^* + 2\,H_2O + 4\,e^- \rightarrow 2\,Pt + 4\,OH^-$, or H_2O in acidic media through $2\,Pt{-}O^* + 4\,H^+ + 4\,e^- \rightarrow 2\,Pt + 2\,H_2O$, under the Pt active species and electric field of the cell, as shown in route 1 in step 2 (Scheme 1). In addition to the above surface route, an alternative lattice route could also be possible. There is abundant lattice oxygen presented in the support $Na_4Ge_9O_{20}$, as proved by the XPS results (Figure S4 a). Those lattice oxygen close to Pt nanoparticles could interact with the surface Pt atoms and thus form the low valence PtO species, as proved by the XPS results (Figure S4 b), which can generate OH^- in alkaline media through $2\,PtO + 2\,H_2O + 4\,e^- \rightarrow 2\,Pt + 4\,OH^-$, or H_2O in acidic media through $2\,PtO + 4\,H^+ + 4\,e^- \rightarrow 2\,Pt + 2\,H_2O$, under the effect of an electric field. Meanwhile, the O_{ads} on the support surface from the external oxygen supply will migrate into the lattice and take the position of initial lattice oxygen ($O_{ads} \rightarrow O_{lattice}$) through the micropore and mesoporous channels of the crystals $Na_4Ge_9O_{20}$, as demonstrated in route 2 in the step 2 (Scheme 1). The two ORR routes indicate that both Pt and PtO as active sites can accelerate the ORR, and the efficient diffusion and migrate of O_2 owing to the special porous structure of the sodium germinate support can also improve the electrocatalysis activity.

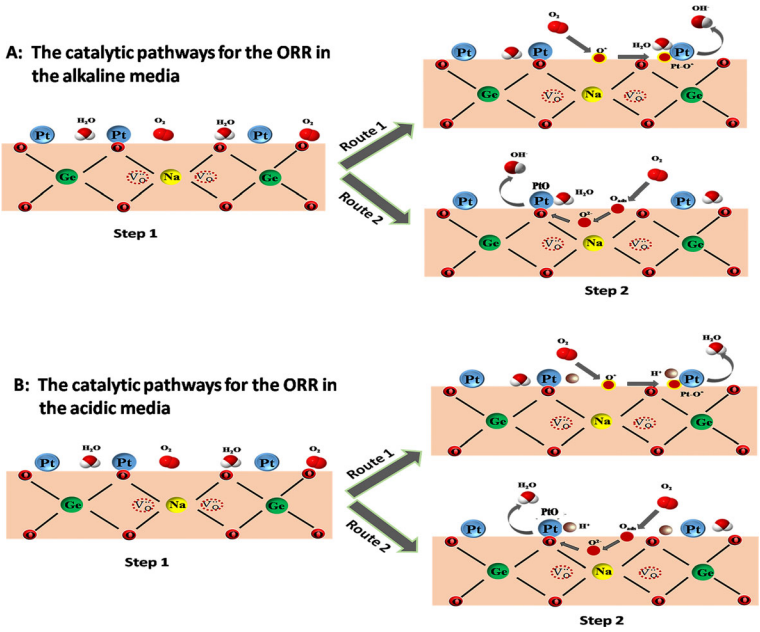

Scheme 1. Schematics for the possible catalytic pathways of ORR on Pt/$Na_4Ge_9O_{20}$ in the alkaline media (A) and acidic media (B). Step 1: the generation of oxygen vacancies and PtO species; Step 2: two routes of the reduction of O_2 in the alkaline media: Route 1 is the surface route in which ambient oxygen molecules are activated to active O* on the support and then form Pt–O* species on Pt NPs, favoring the oxygen reduction; Route 2 is the lattice route in which lattice oxygen migrate to Pt and form PtO species, then the ambient oxygen molecules will be reduced and take the initial positions of latticed oxygen.

Compared to the commercial Pt/C, this new type of electrocatalyst Pt/$Na_4Ge_9O_{20}$ shows approximately 4 and 2-fold increases in the mass activity in acidic and alkaline media, respectively. The excellent catalytic activity can be ascribed to the following aspects: 1) much improved adsorption of ambient O_2 by $Na_4Ge_9O_{20}$ owing to the oxygen vacancies in its lattice, which help the oxygen activation and reduction on Pt nanoparticles;[28] 2) the efficient diffusion of O_2 related to the special porous structure characters of the support; and 3) promoted PtO formation by the lattice oxygen species, through which OH^-/H_2O species are generated through the reaction between H_2O/H^+ and oxygen from PtO. In addition, the uniform and stable dispersion of Pt nanoparticles, the binding of Pt to oxygen species on the surface of the support, and the high structure stability of the $Na_4Ge_9O_{20}$ matrix are also believed to contribute to the excellent durability of the Pt/$Na_4Ge_9O_{20}$ electrocatalyst.

In conclusion, a novel type of low Pt-loaded semiconductor, Pt/$Na_4Ge_9O_{20}$ electrocatalyst, has been synthesized through a facile process, and its electrocatalytic activity toward ORR in both acidic and alkaline electrolyte solutions has been explored for the first time. Such a catalyst with 5 wt% Pt loading shows comparable ORR activities to commercial 20 wt% Pt/C catalyst and follows a four-electron pathway in the acidic and alkaline media (i.e., the ORR mass activity of the Pt/$Na_4Ge_9O_{20}$ is four times and twice that of the commercial 20 wt% Pt/C in acidic and alkaline electrolyte solutions, respectively). More importantly, Pt/$Na_4Ge_9O_{20}$ demonstrates excellent electrochemical durability in the ORR, with its half-wave potentials decayed by only 15 and 20 mV up to 5000th cycle in the alkaline and acidic electrolyte solutions, respectively, in contrast to the commercial 20 wt% Pt/C. This study confirms that the co-existence of highly dispersed Pt and PtO on the support $Na_4Ge_9O_{20}$ in this catalyst system should be responsible for the enhanced catalytic activity and excellent durability. The study is also beneficial for the exploration of highly efficient, low Pt loading and non-carbonaceous electrocatalysts.

Acknowledgements

This research was sponsored by the National Key Basic Research Program of China, (2013CB933200), China National Funds for Distinguished Young Scientists (51225202) and National Natural Science Foundation of China (51502330).

Keywords: electrocatalyst · fuel cells · oxygen reduction reaction · platinum · sodium germanate

[1] M. T. Islam, S. A. Shahir, T. M. I. Uddin, A. Z. A. Saifullah, *Renewable Sustainable Energy Rev.* **2014**, *39*, 1074.
[2] Y.-J. Wang, D. P. Wilkinson, J. Zhang, *Chem. Rev.* **2011**, *111*, 7625.
[3] U. Paulus, A. Wokaun, G. Scherer, T. Schmidt, V. Stamenkovic, V. Radmilovic, N. Markovic, P. Ross, *J. Phys. Chem. B* **2002**, *106*, 4181.
[4] S. I. Choi, S. Xie, M. Shao, N. Lu, S. Guerrero, J. H. Odell, J. Park, J. Wang, M. J. Kim, Y. Xia, *ChemSusChem* **2014**, *7*, 1476.
[5] X. Zhao, S. Chen, Z. Fang, J. Ding, W. Sang, Y. Wang, J. Zhao, Z. Peng, J. Zeng, *J. Am. Chem. Soc.* **2015**, *137*, 2804.
[6] M. Watanabe, D. A. Tryk, M. Wakisaka, H. Yano, H. Uchida, *Electrochim. Acta* **2012**, *84*, 187.
[7] Y. S. Kim, S. H. Jeon, A. Bostwick, E. Rotenberg, P. N. Ross, V. R. Stamenkovic, N. M. Markovic, T. W. Noh, S. Han, B. S. Mun, *Adv. Energy Mater.* **2013**, *3*, 1257.
[8] N. Todoroki, T. Kato, T. Hayashi, S. Takahashi, T. Wadayama, *ACS Catal.* **2015**, *5*, 2209.
[9] J. Kibsgaard, Y. Gorlin, Z. Chen, T. F. Jaramillo, *J. Am. Chem. Soc.* **2012**, *134*, 7758.
[10] L. Yang, S. Jiang, Y. Zhao, L. Zhu, S. Chen, X. Wang, Q. Wu, J. Ma, Y. Ma, Z. Hu, *Angew. Chem.* **2011**, *123*, 7270.
[11] W. Wei, Y. Tao, W. Lv, F. Y. Su, L. Ke, J. Li, D. W. Wang, B. Li, F. Kang, Q. H. Yang, *Sci. Rep.* **2014**, *4*, 6289.
[12] Y. Liang, Y. Li, H. Wang, J. Zhou, J. Wang, T. Regier, H. Dai, *Nat. Mater.* **2011**, *10*, 780.
[13] C. Zhang, N. Mahmood, H. Yin, F. Liu, Y. Hou, *Adv. Mater.* **2013**, *25*, 4932.
[14] Z. Ma, S. Dou, A. Shen, L. Tao, L. Dai, S. Wang, *Angew. Chem.* **2015**, *127*, 1908.
[15] L. Lai, J. R. Potts, D. Zhan, L. Wang, C. K. Poh, C. Tang, H. Gong, Z. Shen, J. Lin, R. S. Ruoff, *Energy Environ. Sci.* **2012**, *5*, 7936.
[16] F. Cheng, J. Shen, B. Peng, Y. Pan, Z. Tao, J. Chen, *Nat. Chem.* **2011**, *3*, 79.
[17] M. Kumar, R. Awasthi, A. Sinha, R. Singh, *Int. J. Hydrogen Energy* **2011**, *36*, 8831.
[18] G. Ilyushin, L. Dem'yanets, *Crystallogr. Rep.* **2003**, *48*, 888.
[19] F. Wang, Y. Jiang, D. J. Lawes, G. E. Ball, C. Zhou, Z. Liu, *ACS Catal.* **2015**, *5*, 3924.
[20] A. Hassan, V. A. Paganin, E. A. Ticianelli, *Appl. Catal. B* **2015**, *165*, 611.
[21] M. Ni, M. K. Leung, D. Y. Leung, K. Sumathy, *Energy Rev.* **2007**, *11*, 401.
[22] J. Shi, *Chem. Rev.* **2013**, *113*, 2139.
[23] M. Woodhouse, B. Parkinson, *Chem. Soc. Rev.* **2009**, *38*, 197.
[24] A. S. Aricò, A. K. Shukla, H. Kim, S. Park, M. Min, V. Antonucci, *Appl. Surf. Sci.* **2001**, *172*, 33.
[25] K. Prabhakaran, T. Ogino, *Surf. Sci.* **1995**, *325*, 263.
[26] K. Kuribayashi, S. Kitamura, *Thin Solid Films* **2001**, *400*, 160.
[27] U. A. Paulus, T. J. Schmidt, H. A. Gasteiger, R. J. Behm, *J. Electroanal. Chem.* **2001**, *495*, 134.
[28] S. Schäfer, S. A. Wyrzgol, R. Caterino, A. Jentys, S. J. Schoell, M. Hävecker, A. Knop-Gericke, J. A. Lercher, I. D. Sharp, M. Stutzmann, *J. Am. Chem. Soc.* **2012**, *134*, 12528.

Received: June 12, 2016
Revised: July 2, 2016
Published online on ■■ ■■, 0000

Less Pt, higher activity: A Pt(5 wt%)/$Na_4Ge_9O_{20}$ composite shows not only high electrochemical catalytic activity for the oxygen reduction reaction (ORR), but also remarkably enhanced Pt mass-specified ORR current density in both acidic and alkaline electrolyte media, which are comparable to those of the commercial Pt/C catalyst.

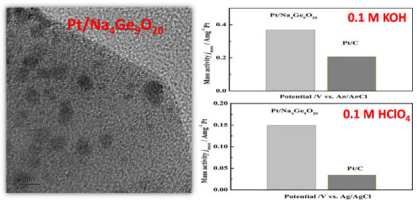

X. Zhou, L. Chen, G. Wan, Y. Chen, Q. Kong, H. Chen, J. Shi**

■■ – ■■

Low Pt-Loaded Mesoporous Sodium Germanate as a High-Performance Electrocatalyst for the Oxygen Reduction Reaction